Dynamic gene expression by putative hair-cell progenitors during regeneration in the zebrafish lateral line

Aaron B. Steiner[1], Taeryn Kim, Victoria Cabot[2], and A. J. Hudspeth

Howard Hughes Medical Institute and Laboratory of Sensory Neuroscience, The Rockefeller University, New York, NY 10065

Edited* by Yuh Nung Jan, Howard Hughes Medical Institute, University of California, San Francisco, CA, and approved February 25, 2014 (received for review October 2, 2013)

Hearing loss is most commonly caused by the destruction of mechanosensory hair cells in the ear. This condition is usually permanent: Despite the presence of putative hair-cell progenitors in the cochlea, hair cells are not naturally replenished in adult mammals. Unlike those of the mammalian ear, the progenitor cells of nonmammalian vertebrates can regenerate hair cells throughout life. The basis of this difference remains largely unexplored but may lie in molecular dissimilarities that affect how progenitors respond to hair-cell death. To approach this issue, we analyzed gene expression in hair-cell progenitors of the lateral-line system. We developed a transgenic line of zebrafish that expresses a red fluorescent protein in the presumptive hair-cell progenitors known as mantle cells. Fluorescence-activated cell sorting from the skins of transgenic larvae, followed by microarray-based expression analysis, revealed a constellation of transcripts that are specifically enriched in these cells. Gene expression analysis after hair-cell ablation uncovered a cohort of genes that are differentially regulated early in regeneration, suggesting possible roles in the response of progenitors to hair-cell death. These results provide a resource for studying hair-cell regeneration and the biology of sensory progenitor cells.

alkaline phosphatase | auditory | neuromast | supporting cell

Because the mammalian auditory epithelium is normally incapable of regeneration, hair-cell death in the inner ear causes irreversible hearing loss. This lack of regenerative capacity is at odds with evidence that multipotent progenitor cells reside in the mammalian cochlea and can produce hair cells under appropriate conditions in vitro (1–4). Unlike those cells of the mammalian ear, progenitor cells in nonmammalian vertebrates readily regenerate hair cells throughout life (5, 6). It has been proposed that this difference reflects greater structural constraints on cells in the sensory epithelia of mammals than on those in other vertebrates (7–9). An alternative hypothesis is that nonmammalian progenitor cells retain responsiveness to signs of hair-cell death, such as intercellular signals, that has been lost in mammals. Detailed characterization of progenitor cells from nonmammalian vertebrates may therefore reveal molecular differences that affect regenerative potential, providing clues as to how regeneration could be conferred on the mammalian ear.

Mantle cells constitute a population of hair-cell progenitors in the zebrafish lateral line, a sensory system comprising organs called neuromasts that detect motion in the aquatic environment. Some mantle cells are mitotically active in the steady state, with many more entering S phase shortly after hair-cell ablation (10, 11). Mantle cells of the most caudal neuromasts react similarly upon tail amputation, entering the cell cycle and contributing to the growth of new neuromasts on the regenerating caudal fin (12). Mantle cells are also contiguous to interneuromast cells that connect adjacent neuromasts and proliferate to produce neuromasts de novo throughout larval development (13, 14). The responsiveness of mantle cells to hair-cell death makes them a useful model for identifying genes that control the initiation of regeneration. Only a few molecular markers for these cells have been identified, however, and even fewer have been confirmed as mantle cell-specific (15–17).

Although previous transcriptomic screens have sought genes expressed in the lateral line, none has focused on mantle cells (18–20). The results of such studies reflect gene expression in several cell types, a complication that might mask gene expression in progenitors. One factor impeding the isolation and characterization of progenitor cells has been the lack of a transgenic line in which these cells are inclusively and specifically labeled, allowing their separation by cell sorting. The only line described to date that expresses a fluorescent protein specifically in mantle cells, *Et*(*krt4:EGFP*)*sqEt20* (hereafter referred to as *Et20*), exhibits gaps in expression indicating that some cells remain unlabeled (21, 22). We have therefore developed a line of transgenic zebrafish that expresses a fluorescent protein in mantle cells more inclusively and have used a transcriptomic approach to reveal genes that are enriched in mantle cells.

Results

***Tg*(*−4.7alpl:mCherry*) Transgenic Zebrafish Express a Red Fluorescent Protein in Mantle Cells.** Several studies indicate that the progeny of mantle cells do not directly become hair cells, but instead transit through at least one intermediate phase before their terminal

Significance

Hearing impairment is most frequently caused by the loss of sensory hair cells in the cochlea. One potential means of alleviating hearing loss is to restore these cells, which do not naturally regenerate in mammals. The zebrafish lateral line serves as a useful model for studying hair-cell regeneration because in this system there exist progenitors, mantle cells, from which hair-cell precursors originate. We have produced zebrafish with fluorescently labeled mantle cells, isolated those cells by flow cytometry, and analyzed the transcripts that they express. We have also defined the temporal window during which mantle cells respond to hair-cell death. This approach has identified genes representing unexpected signaling pathways that may contribute to the development of treatments for hearing loss.

Author contributions: A.B.S., T.K., V.C., and A.J.H. designed research; A.B.S., T.K., and V.C. performed research; A.B.S., T.K., and V.C. analyzed data; and A.B.S. and A.J.H. wrote the paper.

The authors declare no conflict of interest.

Freely available online through the PNAS open access option.

Data deposition: The data reported in this paper have been deposited in the Gene Expression Omnibus (GEO) database, www.ncbi.nlm.nih.gov/geo (accession no. GSE55853).

*This Direct Submission article had a prearranged editor.

[1]To whom correspondence should be addressed. E-mail: asteiner@rockefeller.edu.

[2]Present address: Department of Molecular Biology, Cell Biology, and Biochemistry, Brown University, Providence, RI 02912.

This article contains supporting information online at www.pnas.org/lookup/suppl/doi:10.1073/pnas.1318692111/-/DCSupplemental.

division and differentiation (10, 22–24). The regions of the neuromast in which these immediate hair-cell precursors arise are marked by endogenous alkaline phosphatase activity (24–26). Expecting that the control elements of the cognate gene would drive reporter-gene expression in this subset of cells, we identified the gene responsible for this activity, liver/bone/kidney alkaline phosphatase (*alpl*), and cloned a 4.7-kb portion of its enhancer. However, the *Tg*(*–4.7alpl:mCherry*) transgenic larvae (hereafter termed *alpl:mCherry*) in which this enhancer drives expression of the fluorescent protein mCherry instead display red fluorescence in a pattern suggestive of mantle cells and their associated interneuromast cells, along with weak expression in other tissues including some fin and pigment cells. When the *alpl:mCherry* transgene is crossed into the *Et20* line, mCherry expression in both mantle and interneuromast cells overlaps extensively with the expression of GFP (Fig. 1*A*). The unexpected expression pattern might reflect a position effect on the inserted transgene; alternatively, crucial regulatory elements might lie outside the 4.7-kb fragment of the *alpl* enhancer. Because shared transgene expression makes mantle and interneuromast cells indistinguishable for the purposes of this study, we shall hereafter refer to the combined cell population as mantle cells.

By examining the expression pattern of *alpl:mCherry* larvae relative to those of previously described reporter lines, we confirmed that the transgene specifically and inclusively labels mantle cells (Fig. 1*B*). Crossing to the *Tg*(*–8.0cldnb:lynEGFP*) *zf106* line, in which all neuromast cells express membrane-tethered GFP (27), showed that mCherry occurs only in a subset of cells at each neuromast's periphery (Fig. 1*C*). *alpl:mCherry* is entirely excluded from the sensory cells at the center of the neuromast (Fig. 1*D*), as demonstrated by combination with the *Tg*(*pou4f3:GAP-GFP*) line (hereafter termed *pou4f3:GFP*) that expresses GFP in hair cells (28). A closer inspection of doubly transgenic *alpl:mCherry*;*Et20* larvae verified that the *alpl:mCherry* transgene, like *Et20*, is expressed in mantle and interneuromast cells (Fig. 1*E*). However, we frequently observed one or two peripheral cells per neuromast with mantle cell-like morphology that were labeled with mCherry but not with GFP (Fig. 1*E*). Quantification in 14 neuromasts revealed significantly more mCherry-positive mantle cells per neuromast (11.1 ± 2.1) than GFP-positive mantle cells (10.5 ± 2.2; $P < 0.03$). Assuming that mantle cells can be defined by morphology and position within a neuromast, the *alpl:mCherry* transgene provides a more inclusive fluorescent label for mantle cells than does *Et20*.

***alpl:mCherry* Expression Permits the Isolation of Mantle Cells.** We sought to segregate mantle cells by fluorescence-activated cell sorting (FACS) and to compare their transcriptional profile with those of hair cells and nonsensory epithelial cells. Doubly transgenic *alpl:mCherry*;*pou4f3:GFP* larvae, in which mantle and hair cells were labeled with mCherry and GFP, respectively, were used for sorting of all three populations from the same dissociated tissue. In preliminary experiments, we observed that particles of variable fluorescent brightness, presumably autofluorescent or weakly expressing cells, made it difficult to distinguish highly fluorescent cells from nonfluorescent (NF) epidermal cells. We found that dissecting the skins, to which neuromasts and interneuromast cells remained attached, and using only this material for dissociation and sorting improved the separation of distinct cell populations (Fig. 2*A* and Fig. S1*A*).

Sorting cells from the skins of *alpl:mCherry*;*pou4f3:GFP* larvae yielded two distinct fluorescent populations: one mCherry-positive and GFP-negative (mCh^+), corresponding to putative mantle cells, and the other GFP-positive and mCherry-negative (GFP^+), corresponding to putative hair cells (Fig. 2*B*). To verify that the mCh^+ cell population collected by FACS included the mCherry-positive cells that we had observed by microscopy in the lateral line, we sorted cells from the skins of *alpl:mCherry*;*Et20* transgenic larvae in which most mantle cells were doubly labeled with GFP and mCherry (Fig. 1*E*). We observed a robust rightward shift of mCh^+ cells along the abscissa, indicating coexpression of GFP and mCherry in a subset of cells that were likely mantle cells (hereafter mCh^+/GFP^+) (Fig. 2*C*). Despite the material remaining in the mCh^+/GFP^- quadrant, which likely included fin cells and mCherry-positive, GFP-negative mantle cells (Fig. 1*E*), this result indicated a 12-fold enrichment for mantle cells in the mCh^+ population with respect to total skin cells (20.3% vs. 1.6%).

The mCh^+ cells, GFP^+ cells, and NF skin cells collected from *alpl:mCherry*;*pou4f3:GFP* larvae were subjected to transcriptional analysis on whole-transcriptome microarrays. mCh^+/GFP^+ cells

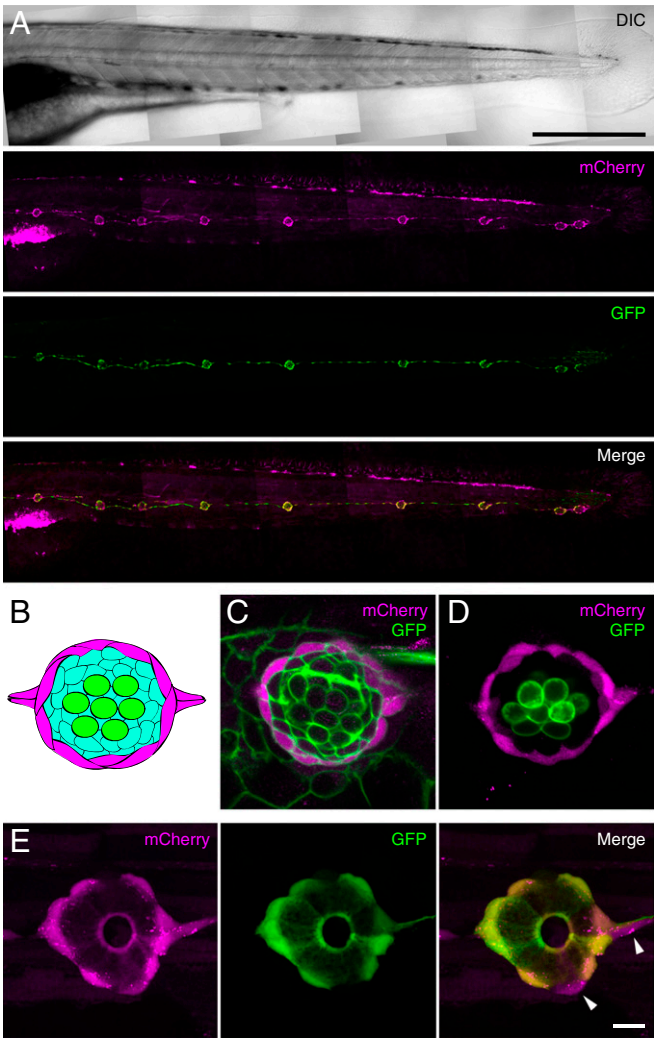

Fig. 1. Expression of fluorescent proteins in mantle cells of the posterior lateral-line system. (*A*) Confocal mosaic images of a living *alpl:mCherry*;*Et20* larva at 4 days postfertilization (dpf) demonstrate expression of mCherry (magenta) overlapping with that of GFP (green) in neuromasts and interneuromast cells. (Scale bar: 500 μm.) The same color code applies in *C–E*. (*B*) A neuromast comprises at least three cell types: hair cells (green), supporting cells (aqua), and mantle cells (magenta). (*C*) mCherry expression in *alpl:mCherry* larvae is limited to a subset of cells at the periphery of the neuromast. The image represents a confocal slice through a living *alpl:mCherry*;*Tg*(*–8.0cldnb:lynEGFP*)*zf106* larva, in which all cells of the neuromast express membrane-tethered GFP. (*D*) An *alpl:mCherry*;*pou4f3:GFP* animal expresses mCherry in peripheral cells, but that marker is excluded from hair cells that express membrane-tethered GFP instead. (*E*) mCherry and GFP have extensively overlapping but not identical expression patterns in mantle cells of *alpl:mCherry*;*Et20* larvae. The arrowheads indicate two mCh^+, GFP^- cells. (Scale bar: *C–E*, 10 μm.)

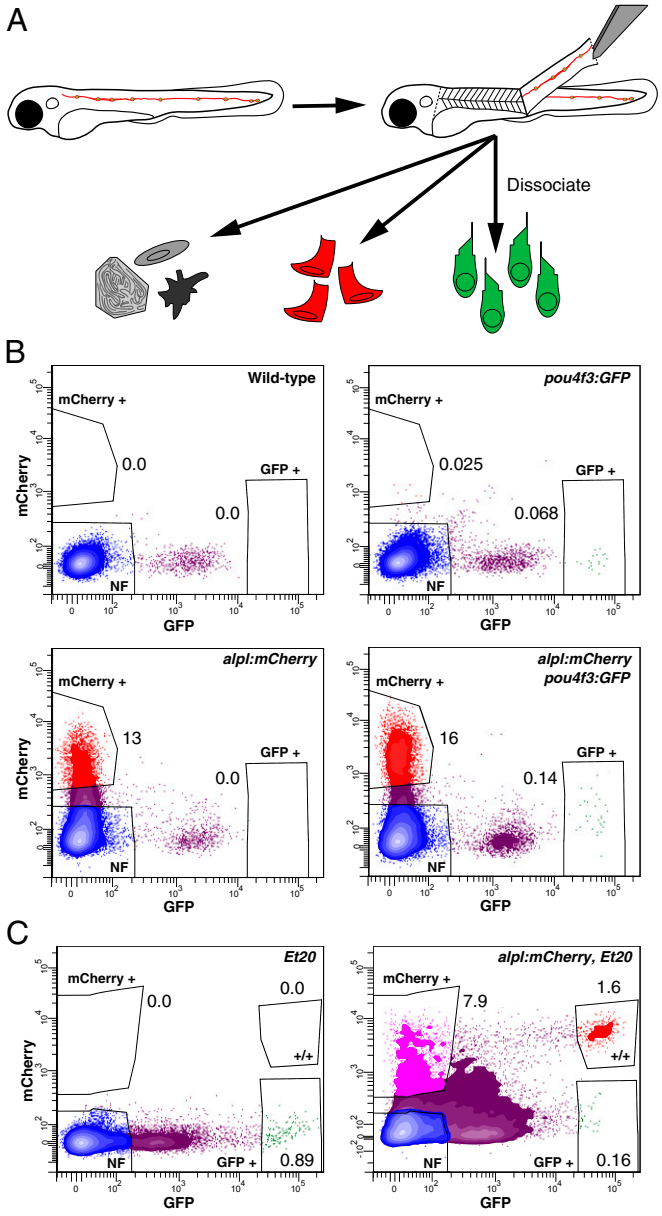

Fig. 2. Isolation of mCherry-expressing mantle cells and GFP-expressing hair cells. (*A*) *alpl:mCherry;pou4f3:GFP* larvae at 4 dpf were terminally anesthetized and their skins were removed with fine forceps. The skins were then dissociated into the component cells, which were sorted by flow cytometry. Red cells represent mCh^+ mantle cells; green cells denote GFP^+ hair cells; and gray and black cells represent epidermal, fin, and pigment cells. (*B*) Representative results from FACS demonstrate the efficient discrimination of GFP^+ (green) and mCh^+ (red) cells from *alpl:mCherry;pou4f3:GFP* larval skins. Each sample included ~50 complete skins. Singly transgenic and nontransgenic controls confirm the selectivity of the gates. (*C*) In plots of the cells sorted from *alpl:mCherry;Et20* larvae, about 20% of mCh^+ cells shifted along the abscissa owing to the dual expression of mCherry and GFP. mCh^+/GFP^- cells are represented here in magenta, whereas red cells are mCh^+/GFP^+. Numbers in plots represent the percentage of total singlet particles within each associated gate.

from *alpl:mCherry;Et20* larvae were also collected and analyzed for comparison (Dataset S1). Principal-component analysis of the results from multiple experiments demonstrated that expressed genes clustered by category (mCh^+, GFP^+, mCh^+/GFP^+, or NF), a result suggestive of consistent sorting (Fig. S2). Although the yield of GFP^+ cells was lower than the observed number of hair cells in the lateral line would suggest, possibly owing to hair cells' sensitivity to dissociation and sorting, pooling multiple sorts provided sufficient material for microarray analysis.

To confirm that the GFP^+ cells were hair cells, we analyzed the biological-process ontology of transcripts expressed at least fivefold as highly in these cells as in NF cells (ANOVA-adjusted $P \leq 0.05$). Consistent with a hair-cell phenotype, transcripts encoding proteins that regulate ciliary assembly and inner-ear stereocilia were among the most enriched (Table 1). Gene-ontology categorization of transcripts enriched at least fivefold in mCh^+ cells accorded with predicted mantle-cell functions. Genes associated with inner-ear morphogenesis and organismal development supported a role for these cells as hair-cell progenitors, and genes in the Wnt pathway accorded with the known role of Wnt signaling in lateral-line development and regeneration (29–34). To ascertain whether mCh^+ mantle cells express a repertoire of genes similar to that of putative progenitor cells from the mammalian cochlea, we sought homologs of genes whose expression is enriched in either of two populations of putative cochlear progenitors. We found that four of 12 homologs enriched in the GFP^-/CD271L/$CD326^+$/CD146L population (3) were significantly enriched in mCh^+ cells with respect to NF cells: *Hes5/her15.1*, *ngfr*, *prox1b*, and *sox2*. Three of the four genes enriched in $Lgr5^+$ hair-cell progenitors (2) were also enriched in mCh^+ cells: *Hes5/her15.1*, *sox2*, and *p27/cdkn1ba*. Although no zebrafish homolog of *Lgr5* has yet been identified, the two analogous genes *lgr4* and *lgr6* were both enriched in mCh^+/GFP^+ cells (Dataset S1).

We used several criteria to select potential mantle cell-specific genes for further study from a list of 2,914 transcripts enriched more than twofold in mCh^+ cells with respect to NF cells (ANOVA-adjusted $P \leq 0.05$; Dataset S2). The degree of enrichment in mCh^+ cells and the statistical significance of this enrichment were the foremost criteria. Genes with greater than twofold enrichment in GFP^+ hair cells with respect to NF cells were eliminated from the list to exclude transcripts enriched in both hair cells and mantle cells, increasing the specificity of our search. Only a single gene enriched in GFP^+ cells, *fndc7*, was retained as a candidate owing to its exceptionally high relative expression in mCh^+ cells (Table 2). Transcripts encoding likely components of signaling pathways not previously implicated in hair-cell regeneration were also considered of particular interest. Several transcripts previously detected in neuromasts by in situ hybridization, including *col17a1b*, *eya1*, *sox2*, and *sox21a*, occurred in our narrowed list of mCh^+ cell-enriched genes, providing evidence that we had successfully captured mantle cells and selected for enriched genes (16, 35–37).

Specific Transcripts Are Expressed in Mantle Cells. Sixteen candidate transcripts, each expressed more highly in mCh^+/GFP^+ mantle cells from *alpl:mCherry;Et20* larvae than in NF cells, were chosen for confirmation by in situ hybridization (Table 2 and Dataset S2). Consistent with the observation that the fin cells of *alpl:mCherry* larvae express low levels of mCherry, six of these transcripts, *c1qtnf5*, *ecrg4a* (*C9H2orf40*), *hpdb*, *pah*, *ptx3b*, and *ucp1*, were found by in situ hybridization to be expressed throughout the medial fin but were not detected in neuromasts. Four other transcripts were expressed in disparate organs and tissues, excluding the fins and neuromasts. However, the six remaining candidates, *fat1a*, *fat1b*, *fgfr1a*, *fndc7*, *robo3*, and *tspan1*, displayed clear expression in neuromasts of the posterior lateral line. Each was expressed most highly in the perimeter of a neuromast, corresponding with the position of mantle cells (Fig. 3*A*). However, not all of the expression patterns were identical. Whereas *fgfr1a* and *fndc7* appeared to be distributed uniformly throughout the periphery, *fat1b* and *tspan1* were restricted to subsets of mantle cells. The signal for *fat1b* predominated in the caudal region of each neuromast, whereas *tspan1* was strikingly localized to the rostral region. The detection of differential

Table 1. Biological-process ontology for transcripts enriched in fluorescently sorted cells

Cell type	Ontological enrichment term	Enrichment score
GFP$^+$ cells		
	Cilium assembly	17.82
	Endocytosis	15.30
	Ciliary or bacterial-type flagellar motility	14.39
	Cilium morphogenesis	12.46
	Detection of mechanical stimulus involved in sensory perception	12.40
	Inner ear receptor stereocilium organization	9.79
	Inner ear morphogenesis	9.20
mCh$^+$ cells		
	Multicellular organismal development	43.41
	Dorsal/ventral pattern formation	22.36
	Wnt receptor signaling pathway	17.13
	Inner ear morphogenesis	15.97
	Aromatic amino acid family metabolic process	15.47
	Fin development	14.68
	Integrin-mediated signaling pathway	13.21

Comparison of gene-ontology enrichment for the biological-process category in GFP$^+$ cells relative to that in NF cells confirms a preponderance of hair cell-associated terms, particularly those related to ciliogenesis. Similar analysis for mCh$^+$ cells shows enrichment of transcripts involved in embryonic development, inner-ear morphogenesis, and Wnt signaling. Gene-ontology analysis was conducted on transcripts expressed at least fivefold as extensively in GFP$^+$ or mCh$^+$ cells as in NF cells ($P \leq 0.05$). Enrichment scores exceeding 3 correspond to $P \leq 0.05$.

gene expression in subsets of mCherry-expressing cells highlights the sensitivity of our approach.

As confirmation of the transcripts enriched in mantle cells, we compared candidate-gene expression with the expression of GFP in *Et20* transgenic larvae by FISH, followed by immunofluorescence for GFP. Because commercially available mCherry antibodies proved inadequate to detect expression of the transgene, we used *Et20* larvae labeled with anti-GFP antibodies rather than *alpl:mCherry* larvae marked with anti-mCherry antibodies in these experiments. The expression of *fat1b* was almost entirely coincident with GFP labeling. Although the expression of *fat1a* and *robo3* exhibited partial overlap with that of GFP, a significant portion of both expression domains lay immediately outside or just inside the ring of GFP expression (Fig. 3*B*). The nonoverlapping regions of expression might reflect expression of these genes in mCh$^+$ cells that do not express GFP in *Et20* larvae. Alternatively, some transcripts that are enriched in mCh$^+$ cells might also occur in a few adjacent NF cells, such as periderm cells surrounding the neuromast. These transcripts would appear to be present in vanishingly small amounts at the population level if present in only a handful of NF cells.

Mantle Cells Exhibit a Transcriptional Response to Hair-Cell Ablation. Having characterized the transcriptional profile of mantle cells in the steady state, we examined their response in the first few hours after the elimination of hair cells. Genes that are differentially

Table 2. Mantle cell-enriched transcripts selected for in situ hybridization

Gene symbol	Gene name	Ensembl transcript identification code	mCh$^+$/NF ratio	GFP$^+$/NF ratio
angpt2b	Angiopoietin 2b	ENSDART00000076023	20.05	0.74
c1qtnf5	C1q and tumor necrosis factor-related protein 5	ENSDART00000078570	11.66	0.13
ecrg4a	Esophageal cancer-related gene 4a (*C9H2orf40*)	ENSDART00000078523	18.41	0.24
fat1a	FAT tumor suppressor homolog 1a	ENSDART00000103262	3.03	0.56
fat1b	FAT tumor suppressor homolog 1b	ENSDART00000011953	17.31	1.51
fgfr1a	Fibroblast growth factor receptor 1a	ENSDART00000074774	3.53	0.48
fndc7	Fibronectin type III domain containing 7	ENSDART00000142938	31.95	12.26
gsg1l	Germ cell-specific gene 1-like	ENSDART00000054408	19.63	0.48
hpdb	4-Hydroxyphenylpyruvate dioxygenase b	ENSDART00000066050	11.92	0.05
mtss1la	Metastasis suppressor 1-like a	ENSDART00000124075	19.44	1.37
pah	Phenylalanine hydroxylase	ENSDART00000011943	21.07	0.61
phex	Phosphate-regulating gene with homologues to endopeptidases on the X chromosome	ENSDART00000090010	11.94	0.53
ptx3a	Pentraxin 3, long a	ENSDART00000098673	16.10	0.14
robo3	Roundabout homolog 3	ENSDART00000024778	21.67	0.62
tspan1	Tetraspanin 1	ENSDART00000073757	11.54	1.08
ucp1	Uncoupling protein 1	ENSDART00000038807	30.63	0.47

Evaluation of differential gene expression between mCh$^+$ and NF cells yields a list of candidate mantle cell-enriched genes. Only genes with highly significant enrichment in mCh$^+$ cells ($P < 0.00001$) are included in this list. Conversely, each gene, with the exception of *fndc7*, is either not significantly enriched or is significantly reduced in GFP$^+$ relative to NF cells.

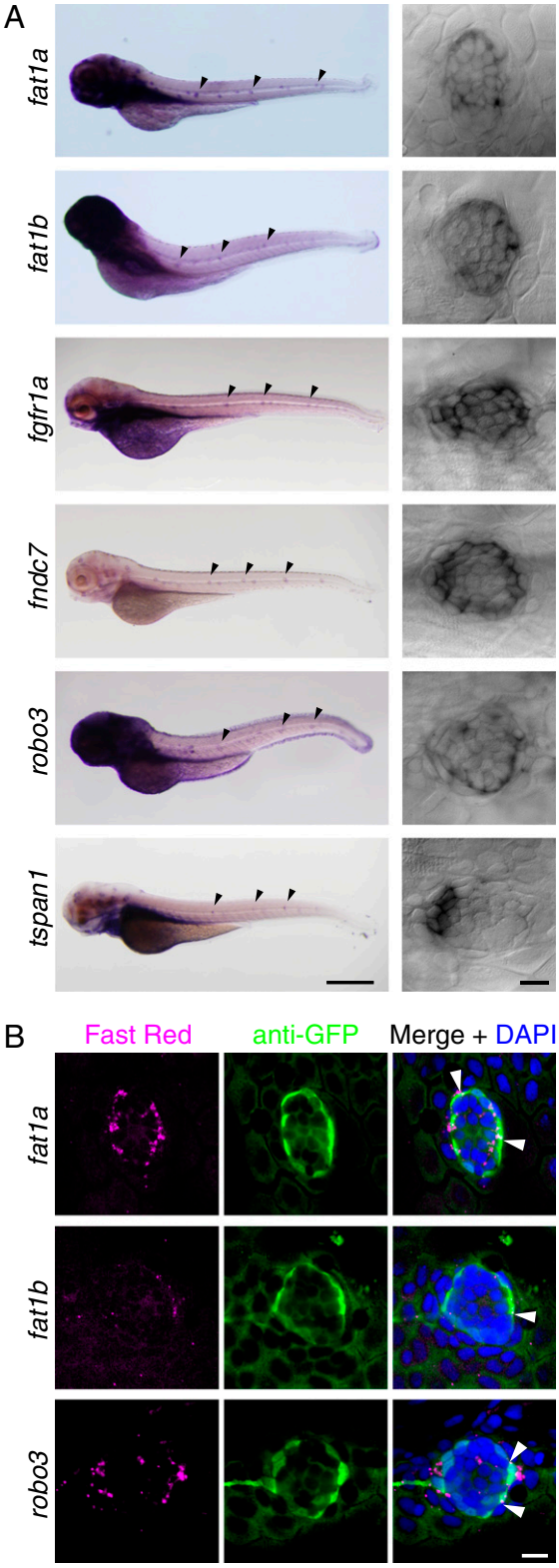

Fig. 3. Confirmation by in situ hybridization of molecular markers for mantle cells. (*A*) As shown in low-magnification micrographs (*Left*; neuromasts indicated by black arrowheads) and confocal differential-interference-contrast images (*Right*), *fat1a*, *fat1b*, *fgfr1a*, *fndc7*, *robo3*, and *tspan1* are expressed in neuromasts of the posterior lateral line. Note that each transcript is most prominent in a subset of cells at the periphery of the neuromast. (Scale bar: *Left*, 500 μm; *Right*, 10 μm.) (*B*) *fat1a*, *fat1b*, and *robo3* each display a pattern of expression distinct from that of the *Et20* transgene. FISH (*Left*; Fast Red) followed by immunofluorescent labeling of GFP (*Middle*) in *Et20* larvae permits the comparison of each transcript's expression pattern with transgenic GFP expression in mantle cells. (*Right*) Nuclei are labeled by DAPI. White arrowheads indicate colocalization of in situ labeling and anti-GFP immunofluorescence. (Scale bar: 10 μm.)

regulated during this period presage the entry of mantle cells into the cell cycle, and may therefore play important roles in initiating hair-cell regeneration. mCh^+ cells and NF cells were isolated from *alpl:mCherry;pou4f3:GFP* larvae 1, 3, 5, and 11 h after hair cells had been extirpated by treating larvae with $CuSO_4$, which has previously been shown to destroy hair cells without damaging mantle cells (38, 39). Flow cytometry confirmed that this treatment rapidly eliminated hair cells (Fig. S1*B*). Genes that showed up- or down-regulation of greater than twofold in NF cells concurrent with a change in the same direction in mCh^+ cells were excluded from further analysis, limiting our scope to mantle cell-specific changes in gene expression (Dataset S3).

We identified 8,569 transcripts whose expression either at least doubled or decreased to less than half compared with untreated controls at one or more of the four collection times (ANOVA-adjusted $P \leq 0.05$; Dataset S4). To identify trends in the changing gene expression, we subjected the temporal expression patterns of these genes to hierarchical clustering analysis, grouping together genes with similar up- and down-regulation over time. Many genes showed the greatest up- or down-regulation at the 3-h and 5-h collection times but were relatively unchanged in their expression levels relative to controls at 1 h and 11 h (Fig. 4*A*). Although not universal among differentially expressed genes, this pattern suggests that transcription in mantle cells changed radically a few hours after hair-cell death but soon reverted to baseline levels.

We selected 10 transcripts for closer examination on the basis of the degree and statistical significance of differential regulation at any time posttreatment with respect to untreated controls. We included representatives of several different temporal expression patterns (Fig. 4*A*). Genes whose expression was initially enriched in mantle cells but decreased after hair-cell death were examined along with those showing increased expression, for either transcriptional repression or activation might affect regeneration (40, 41). For comparison, we included in the resulting heat map the temporal expression patterns of *socs3a*, *socs3b*, and *stat3*, three genes whose expression has been shown to increase in the zebrafish inner ear and lateral line after noise-induced damage (42) (Fig. 4*A*). Our results indicated that these genes underwent a transient increase in expression in mantle cells immediately following hair-cell ablation but that their activity subsequently diminished.

We confirmed the microarray results for selected genes by quantitative PCR (qPCR) analyses. The expression level of each gene was examined at the time after $CuSO_4$ treatment when microarray analysis showed the greatest difference in expression from untreated controls. Thus qPCR analyses for *btr04*, *fat2*, *klf3*, *fgfr1a*, and *prom2* expression were performed at 1 h after $CuSO_4$ treatment, whereas assays for *arpc1a*, *atg2bl*, *fndc7*, *lgals1l*, and *tspan1* were conducted at 3 h after $CuSO_4$ treatment. Values were normalized to the expression levels of a set of reference genes and then compared with those of cells from untreated larvae. Six of the 10 genes displayed changes in expression in the same direction as those determined by microarray analysis, although in most cases the magnitude of change was reduced (Table 3).

To assess the modulation of gene expression visually in mantle cells after hair-cell destruction, we performed in situ hybridization for *fndc7* and *tspan1* either with or without $CuSO_4$ treatment. Both genes were expected from the microarray and qPCR results to decrease in expression after $CuSO_4$ treatment (Fig. 4*A* and Table 3). In situ hybridization 3 h after treatment demonstrated a dramatic reduction, to almost undetectable levels, in the expression of *fndc7* and *tspan1* in mantle cells (Fig. 4*B*).

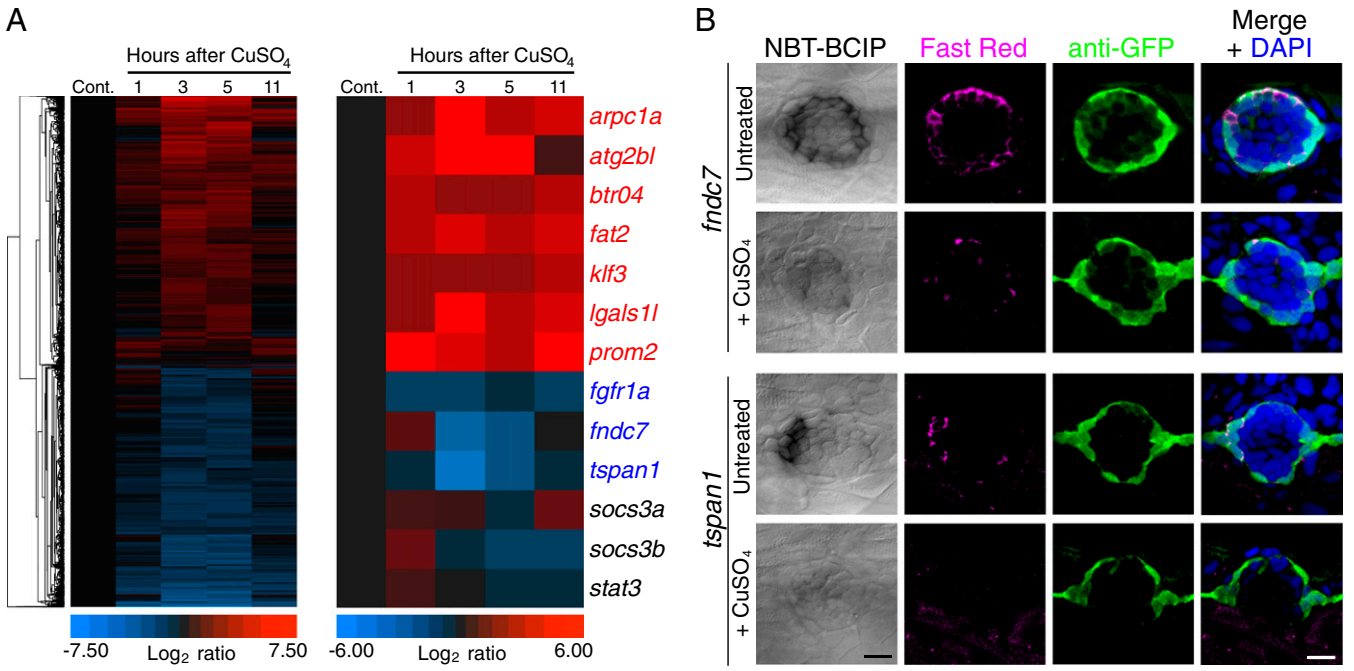

Fig. 4. Transcriptional response of mantle cells to hair-cell destruction. (*A*) Extirpation of hair cells by the ototoxic chemical $CuSO_4$ evokes the dynamic expression of select candidate genes in sorted mCh^+ cells. Microarray results from samples dissected 1, 3, 5, and 11 h after treatment were normalized to those from untreated control samples (*Cont.*). (*Left*) Unsupervised hierarchical clustering of all of the genes whose expression was up- or down-regulated by at least a factor of 2 at some time after treatment, except genes whose expression also changed in NF cells. (*Right*) Genes of interest were selected on the basis of the degree and significance of differential expression as well as the availability of reliable annotation. The genes listed in blue were primarily down-regulated following hair-cell ablation, whereas those shown in red were principally up-regulated. The genes labeled in black were previously reported to be up-regulated in the sound-damaged zebrafish inner ear (42). (*B*) In situ hybridization supports the results from microarrays and reverse-transcription qPCR analyses: Both *fndc7* and *tspan1* are enriched in mantle cells and demonstrate reduced expression following $CuSO_4$ treatment. The first column displays the results of chromogenic in situ hybridization; the second and third columns compare FISH (Fast Red) with GFP immunoreactivity (green) in *Et20* larvae. The merged images in the fourth column include nuclear staining with DAPI (blue). (Scale bars: 10 μm.)

Colabeling for GFP in *Et20*-positive larvae indicated that mantle cells survived $CuSO_4$ treatment, verifying that the reduction in *fndc7* and *tspan1* transcripts did not reflect the loss of the cells that express them.

Discussion

We have used two technical innovations to identify genes whose expression is enriched in putative hair-cell progenitors and characterized the initial transcriptional events preceding the cells' entry into the cell cycle. First, to improve the separation of different cell populations, we used only the dissected skins of larval zebrafish as starting material. We additionally developed the *alpl:mCherry* transgenic line in which mantle cells are fluorescently labeled more inclusively than in *Et20* larvae, the only line described previously with a similar expression pattern. Because they exclude contaminants such as fin cells, mCh^+/GFP^+ mantle cells isolated from *alpl:mCherry;Et20* larvae likely represent a purer population than mCh^+ cells from *alpl:mCherry* animals. We nevertheless focused on transcription in mCh^+ cells to retain mCh^+/GFP^- cells that would otherwise have been discarded (Figs. 1*E* and 2*C*). Because it remains uncertain whether only a subset of mantle cells can act as hair-cell progenitors, it is possible that mCh^+/GFP^- cells represent a rare but important progenitor population.

We identified a number of transcripts whose expression is enriched in mantle cells relative to other cell types in the skin, including hair cells. The overlap in transcript enrichment between mantle cells and putative progenitor cells from two studies of the mammalian cochlea suggests a degree of similarity between

Table 3. Differential expression of candidate genes following $CuSO_4$ treatment

Gene symbol	Gene name	Ensembl or GenBank transcript identification code	$CuSO_4$ treated/untreated ratio
arpc1a	Actin-related protein 2/3 complex, subunit 1A	NM_001002100	7.23 ± 2.94*
atg2bl	Autophagy-related protein 2 homolog B-like	XM_001340472	1.52 ± 0.49
fat2	FAT tumor suppressor homolog 2	ENSDART00000014149	4.99 ± 2.91*
klf3	Krüppel-like factor 3	ENSDART00000014916	1.91 ± 1.07
lgals1l1	Lectin, galactoside-binding, soluble, 1 (galectin 1)-like 1	ENSDART00000141904	11.33 ± 3.78*
tspan1	Tetraspanin 1	ENSDART00000073757	0.01 ± 0.08*

klf3, *fat2*, and *tspan1* were assayed 1 h after $CuSO_4$ treatment, whereas *arpc1a*, *atg2bl*, and *lgals1l1* were assayed 3 h after exposure. Each value was normalized to that for the reference gene *slc25a5* and expressed as a ratio to its own expression under control conditions. Values are given with SEMs.
*$P < 0.05$.

these cell types (2, 3), a result that supports the utility of the lateral line as a model for hair-cell regeneration in the mammalian ear.

All of the transcripts whose enrichment in mantle cells was confirmed by in situ hybridization encode membrane-spanning proteins. It is unclear whether this characteristic reflects an unknown bias in our data collection or analysis, or whether mantle cells preferentially express transmembrane receptors and cell adhesion molecules. High baseline expression of receptor proteins might, for example, underlie the rapid response of mantle cells to signals induced by hair-cell damage. The discovery that *fat1a* and *fat1b* are enriched in mantle cells is particularly interesting in light of the established roles of Fat protocadherins in controlling cell proliferation and organ size in *Drosophila* (43–45). Fat homologs and their partner, Dachsous, are also integral to cell-polarity determination in vertebrate systems, including the mammalian ear, and might be expected to coordinate cellular processes during regeneration (46–48). The possible functions of other receptors enriched in mantle cells are more difficult to predict. For example, Robo3 is generally associated with neuronal growth cones and interacts with Robo receptors to facilitate axonal pathfinding (49–52). Although Robo3 also regulates such diverse activities as the migration of cancer cells and the retraction of apical processes in retinal ganglion cells, it remains unclear how it might function in hair-cell progenitors (53, 54). Still other molecules, such as that encoded by the highly enriched transcript *fndc7*, have not yet been assigned a specific function in any system and may represent novel pathways.

An unexpected outcome of this work is the observation that certain transcripts, particularly *fat1b* and *tspan1*, are restricted to subsets of mantle cells clustered at particular locations within a neuromast. These highly restricted expression domains suggest that mantle cells are subdivided into multiple populations with different transcriptional profiles and perhaps distinct functions. The closely related genes *fat1a* and *fat1b* differ in their expression patterns: *fat1a* transcripts occur uniformly throughout the ring of mantle cells, whereas *fat1b* transcripts localize predominantly to the posterior-most mantle cells within each neuromast (Fig. 3). In mammals, only a single Fat1 protein has been identified; the differential distribution of *fat1a* and *fat1b* transcripts may signal distinct roles for the two paralogs in zebrafish.

Our methodology allowed the analysis of rapid changes in gene expression by mantle cells. Because we used $CuSO_4$ to destroy hair cells, we were able to assay transcription within 1 h of hair-cell death. By collecting cells at closely spaced times thereafter, we captured gene-expression differences with higher temporal resolution than that in previous studies of hair-cell regeneration (42, 55). The importance of high temporal resolution is highlighted by our observation that the most dramatic transcriptional change in mantle cells takes place from 3 h to 5 h after hair-cell death (Fig. 4*A*). This period accords with immediate-early transcriptional responses during regeneration in systems ranging from planarian neoblasts to mammalian hepatocytes, pointing to a commonality in the temporal response to tissue damage (56, 57). As a validation of our approach, we detected increases in the expression of *socs3a*, *socs3b*, and *stat3* consistent with results following noise-induced damage (42).

Genes whose expression in progenitor cells responds to hair-cell death provide a window into how these cells ready themselves for proliferation. For example, the significant up-regulation of genes encoding cytoskeletal regulators such as arpc1a, an Arp2/3 complex component that supports lamellipodium formation, and prom2, which drives filopodial extension, suggests that rearrangements of the actin cytoskeleton precede entry into the cell cycle (58, 59). The transcript encoding the Fat family protein fat2 is also up-regulated, consistent with the possible involvement of Fat signaling in regeneration. Other up-regulated genes suggest less characterized pathways that could affect neuromast recovery; *atg2bl*, for example, is a putative mediator of autophagy, a process only recently implicated in stem-cell maintenance and regeneration (60).

Many transcripts, including those for the fibronectin type III domain-containing protein fndc7 and the tetraspanin family protein tspan1, are down-regulated in mantle cells after $CuSO_4$ treatment (Fig. 4 *A* and *B* and Table 3). The down-regulation of genes in mantle cells during regeneration could prove significant: Proteins that inhibit proliferation may need to be cleared in order for regeneration to proceed, whereas those that stimulate proliferation might be negatively regulated to prevent excessive cell division. Understanding the roles of genes down-regulated in mantle cells during regeneration may help us to comprehend and overcome the inability of endogenous progenitors to regenerate the sensory epithelium in mammals.

A concurrent study published in this issue of PNAS (61) provides a complementary view of gene expression in mantle cells with results largely consistent with those reported here. For example, all six of the transcripts that we confirmed by in situ hybridization to be enriched in mantle cells were also identified by these researchers. Furthermore, nine of the 14 genes we found to be differentially regulated after hair-cell death changed expression in the same direction in the accompanying study. The dissimilarities in the lists of transcripts likely reflect differences in the techniques used by the two groups: the other authors ablated hair cells by treating larvae with the antibiotic neomycin as opposed to $CuSO_4$. They used the *Et20* transgenic line rather than the *alpl:mCherry* line to sort mantle and supporting cells. Finally, they characterized the transcriptional profile of GFP-positive cells by whole-transcriptome sequencing rather than by microarray analysis. A more detailed comparison of the results can be found in the accompanying paper (61).

Our study provides a molecular characterization of hair-cell progenitors in the zebrafish lateral line and demonstrates changes in gene expression in anticipation of hair-cell regeneration. In addition to serving as a resource for the research community interested in hair-cell regeneration, these results may encourage the formulation of new hypotheses to explain why nonmammalian vertebrates can readily regenerate hair cells, whereas mammals cannot.

Materials and Methods

Animal Care and Strains. Experiments were conducted in accordance with guidelines set forth by the Rockefeller University's Institutional Animal Care and Use Committee. Zebrafish were kept under standard conditions essentially as described (62). Embryos were produced by natural pairings and maintained at 28.5 °C in E3 medium (5 mM NaCl, 0.17 mM KCl, 0.33 mM $CaCl_2$, and 0.33 mM $MgSO_4$). To eliminate pigmentation for in situ hybridization experiments, 200 μM 1-phenyl-2-thiourea was added. WT larvae were of the Tupfel long-fin strain. The *Et20*, *Tg*(*–8.0cldnb:lynEGFP*)*zf106*, and *Tg*(*pou4f3:GAP-GFP*) transgenic lines have been described (21, 27, 28). All experiments used larvae at 4 d postfertilization.

Production of the *alpl:mCherry* Transgenic Line. An enhancer fragment from the *alpl* gene was amplified by PCR from zebrafish genomic DNA with the primers 5′-AA**GGTACC**TGCCTCTCCACCTTAAGCTCCTGG-3′ and 5′-AA**CCCGGG**TTAGGACCCCGGTCACATGGAGC-3′, in which the successive bold-faced sequences indicate KpnI and XmaI recognition sites. The resulting 4.7-kb fragment was cloned into pCR-XL-TOPO (Invitrogen Corp.), digested with KpnI and XmaI, and subcloned into the Tol2kit 5′ entry vector p5E-MCS. The complete plasmid for transgenesis was constructed by recombining the *alpl* enhancer 5′ entry vector with existing Tol2kit plasmids as described (63). This construct was injected into single-cell embryos with mRNA encoding the Tol2 transposase, each at 25 ng/μL. Larvae expressing mCherry were raised to adulthood and screened for germ-line transmission of the transgene.

Live Imaging and Cell Counting. Larvae were anesthetized in 600 μM 3-aminobenzoic acid ethyl ester methanesulfonate in E3 medium and mounted in a 35-mm glass-bottomed chamber under 0.8% low-melting-point agarose containing anesthetic. Confocal imaging was performed with an Olympus IX81 microscope equipped with a Fluoview FV1000 laser-scanning system (Olympus America). After Z-stacks had been acquired at 1-μm intervals,

either representative slices were selected for display or maximum-intensity Z-projections were prepared to demonstrate transgene expression. For mantle-cell counts, *alpl:mCherry;Et20* larvae were mounted and imaged as described above. In each of four larvae, the mCh^+ or GFP^+ cells were counted in the rostral-most four neuromasts deposited by the first primordium. Cells were considered positive for fluorescence if their overall fluorescence level was approximately equal to that of the brightest cell in the neuromast. The statistical significance of cell counts was determined with a Student's *t* test. Adjustments for brightness and contrast, Z-projections, stitching of Z-stacks for mosaic images, and image analysis were performed in Fiji (National Institutes of Health).

Cell Preparation and Flow Cytometry. Immediately before dissection, larvae were anesthetized in 600 μM 3-aminobenzoic acid ethyl ester methanesulfonate in Ringer's solution (116 mM NaCl, 2.6 mM KCl, 1.8 mM $CaCl_2$, and 5 mM Hepes at pH 7.0). Skins were removed with a pair of fine forceps (Dumont no. 5; Fine Science Tools). Each larva was first positioned in one compartment of a three-well, fluorocarbon-coated slide and punctured with a pair of forceps just rostral to the yolk sac and caudal to the heart. The skin at the incision point was grasped with a second pair of forceps and pulled away from the body at an angle of 45°. In most cases, this technique removed the skin from both sides of the larva in one piece.

Dissected skins were immediately transferred to ice-cold Ringer's solution until dissociation. Approximately 50 skins were dissociated for each flow cytometry experiment, and each analysis was conducted at least four times. To obtain sufficient RNA for amplification, we pooled multiple collections of GFP^+ hair cells or mCh^+/GFP^+ mantle cells. For experiments in which gene expression was assessed after hair-cell ablation, larvae were placed in 5 μM $CuSO_4$ for 1 h at 28.5 °C and briefly rinsed in three changes of E3 medium. Their skins were then collected 1, 3, 5, or 11 h later. Treatment with similar concentrations of $CuSO_4$ specifically destroys hair cells but leaves supporting and mantle cells intact (38).

To dissociate skins for cell sorting, we replaced Ringer's solution with 0.25% trypsin-EDTA (Life Technologies) and incubated samples for 15 min in a water bath at 28.5 °C. The samples were then triturated with a P1000 pipet five times or until visibly homogenized. After the trypsin digestion had been quenched with 30% (wt/vol) FBS and 6 mM $CaCl_2$ in PBS solution, the liberated cells were recovered by centrifugation (400 × *g* for 5 min at 4 °C). The pellet was rinsed once with Ca^{2+}-free Ringer's solution containing 0.5 mg/mL DNaseI (Sigma), resedimented by centrifugation, and resuspended in 100 μL of the same solution. The suspension was kept on ice until just before sorting, when it was passed once through a 40-μm filter.

Cells were sorted in a flow cytometer equipped with an 85-μm nozzle and 488-nm and 561-nm lasers (FACSAria II; BD Biosciences). Distinct populations of cells were isolated on the basis of forward scattering, lateral scattering, and the intensity of mCherry or GFP fluorescence. Sorted cells were collected in a lysis-buffer solution (RNeasy Micro Kit; Qiagen) supplemented with 130 mM β-mercaptoethanol and were stored at −80 °C until RNA extraction.

RNA Extraction, Amplification, and cDNA Library Preparation. Total RNA was isolated by a standard protocol (RNeasy Micro Kit; Qiagen). The yield and quality of the product were measured with a spectrophotometer (NanoDrop 1000; NanoDrop Technologies) and a bioanalyzer (Agilent 2100), respectively. Only samples with an RNA integrity score greater than 8.0 were selected for the preparation of cDNA libraries. One nanogram of total RNA from each sample was amplified to several micrograms of cDNA (Pico WTA System V2; NuGEN, Inc.), which was labeled with biotin (Encore Biotin Module; NuGEN, Inc.). The cDNA libraries were assayed for concentration and fragment size with the spectrophotometer and bioanalyzer before and after biotin labeling.

Microarrays and Data Analysis. To assess relative gene expression we used gene chips (Zebrafish Gene 1.0 ST Arrays; Affymetrix) bearing oligonucleotide probes representing more than 59,000 putative transcripts. Because many probes had not been assigned to specific genes or transcripts, we annotated as many as possible using the Ensembl (www.ensembl.org) and National Center for Biotechnology Information Nucleotide (www.ncbi.nlm.nih.gov/nucleotide/) public databases. Biotin-labeled cDNA from each sample was hybridized according to standard protocols. We have deposited the raw microarray data in the Gene Expression Omnibus (www.ncbi.nlm.nih.gov/geo).

The data were first transformed using robust multiarray average normalization (Genomics Suite; Partek). Principal-components analysis was used to identify and discard outliers within each experimental group. At least three independent experiments contributed to each result presented. Because experiments were not always performed or microarrays scanned on the same day, we adjusted all data for batch effects. The statistical significance of differences in gene expression between sample types was evaluated by ANOVA followed by false-discovery-rate control through the Benjamini–Hochberg procedure. Only genes whose changes in expression demonstrated a controlled $P < 0.05$ were considered for further analysis, including ontological classification. We assessed hierarchical clustering of differential-expression profiles after hair-cell ablation by unsupervised Euclidean similarity. Only genes whose expression in mCh^+ cells changed at least twofold at one or more times after $CuSO_4$ treatment were included in this analysis.

Whole-Mount in Situ Hybridization and Imaging. Fragments of the *c1qtnf5*, *ecrg4a*, *fgfr1a*, *fndc7*, *gsg1l*, *mtssl1a*, *phex*, *ptx3b*, *tspan1*, and *ucp1* genes were amplified by PCRs from dissected-skin cDNA. Amplicons were cloned into the pCRII-TOPO vector (Dual-Promoter TOPO TA Cloning Kit; Invitrogen Corp.). Plasmids containing fragments of *angpt2*, *fat1a*, *fat1b*, and *robo3* were gifts, and those containing *hpdb* and *pah* fragments were purchased from commercial suppliers. Primer sequences for cDNA amplification, as well as the sources of externally obtained constructs, are detailed in Table S1. Plasmids were linearized by restriction digestion and purified by phenol-chloroform extraction and ethanol precipitation. About 0.5 μg of linearized DNA template served as the starting material for the synthesis of each sense and antisense riboprobe (SP6/T7 DIG RNA labeling kit; Roche Applied Science). Probe integrity was confirmed by agarose-gel electrophoresis before use.

In situ hybridization was performed according to published protocols (62, 64) with a slight modification to preserve tissue structure: the enzymatic digestion of larvae was reduced to 17 min at room temperature in 2 μg/mL proteinase K. For each antisense riboprobe hybridization, sense probe hybridization was carried out simultaneously as a negative control. Preparation of larvae and hybridization were conducted as above for sequential in situ hybridization and immunofluorescent labeling. These larvae were developed with fluorescent Fast Red substrate as opposed to a conventional chromogenic substrate. After labeling, larvae were rinsed four times in PBS with 0.1% Tween-20, reblocked, and incubated overnight at 4 °C in a 1:500 dilution of purified rabbit anti-GFP antiserum (Torrey Pines Biolabs, Inc.). The secondary antiserum for fluorescent labeling was Alexa Fluor 488 goat anti-rabbit IgG diluted 1:500, and larvae were counterstained with DAPI to label nuclei.

For low-magnification, whole-animal imaging, larvae were mounted in 70% glycerol and 30% PBS. These specimens were imaged with an Olympus DP71 camera mounted on an Olympus SZX7 dissecting microscope. For higher-magnification and fluorescence imaging, larvae were mounted in Vectashield (Vector Laboratories, Inc.). In most cases, the head and yolk were removed to facilitate mounting. Confocal imaging was performed with an Olympus IX81 microscope and Fluoview FV1000 laser-scanning system. Conventionally-stained samples were imaged in confocal differential-interference-contrast mode with a 488-nm laser, whereas combined in situ hybridization- and immunofluorescence-labeled samples were imaged for fluorescence with 405-nm, 488-nm, and 561-nm lasers. All image processing was performed in Fiji (National Institutes of Health).

qRT-PCR Analysis. The NormFinder application was used to select optimal reference genes for our experiments, *β-actin2*, *ef1α*, and *slc25a5*, from a panel curated from the literature (65–67). Most of the primers for qPCR analyses were designed with the online tool National Center for Biotechnology Information Primer-BLAST (www.ncbi.nlm.nih.gov/tools/primer-blast). Those targeting *β-actin1* and *ef1α* were taken from published sequences (67). The sequences for all primers used in qPCR analyses can be found in Table S2. Each primer set was tested for amplification efficiency before use. The amplified cDNA libraries used for microarray hybridization provided templates for qPCR; ∼7.5 ng of cDNA was used per reaction. The data in Table 3 represent the results of at least three analyses, each of which was replicated once. The qPCR analyses were performed on an Applied Biosystems 7900HT Sequence Detection System with FastStart Universal SYBR Green Master mix (Roche Applied Science). Statistical analysis was carried out with a custom-written Python script.

ACKNOWLEDGMENTS. We thank L. Jiang, A. Romero-Carvajal, J. Haug, C. Seidel, and T. Piotrowski for sharing their unpublished results. We thank V. Korzh, D. Gilmour, and H. Baier for providing transgenic zebrafish; L. Goodrich, B. Weinstein, and C. Beattie for plasmids; A. Jacobo for writing the programs for statistical analysis; A. Afolalu and N. McKenney for maintaining fish lines; and our group's members for comments on the manuscript. We also thank members of The Rockefeller University's Genomics and Flow Cytometry Resource Centers. A.B.S. was supported by a Rena Shulsky Fellowship, the F. M. Kirby Foundation, Howard Hughes Medical Institute, and Grant DC00241 from the National Institutes of Health (NIH). V.C. was supported by the F. M. Kirby Foundation and NIH Grant DC10609. T.K. is a Research Technician and A.J.H. is an Investigator of Howard Hughes Medical Institute.

1. Li H, Liu H, Heller S (2003) Pluripotent stem cells from the adult mouse inner ear. *Nat Med* 9(10):1293–1299.
2. Shi F, Kempfle JS, Edge AS (2012) Wnt-responsive Lgr5-expressing stem cells are hair cell progenitors in the cochlea. *J Neurosci* 32(28):9639–9648.
3. Sinkkonen ST, et al. (2011) Intrinsic regenerative potential of murine cochlear supporting cells. *Sci Rep* 1:26.
4. Jan TA, et al. (2013) Tympanic border cells are Wnt-responsive and can act as progenitors for postnatal mouse cochlear cells. *Development* 140(6):1196–1206.
5. Ryals BM, Rubel EW (1988) Hair cell regeneration after acoustic trauma in adult Coturnix quail. *Science* 240(4860):1774–1776.
6. Ryals BM, Westbrook EW (1990) Hair cell regeneration in senescent quail. *Hear Res* 50(1-2):87–96.
7. Burns JC, Collado MS, Oliver ER, Corwin JT (2013) Specializations of intercellular junctions are associated with the presence and absence of hair cell regeneration in ears from six vertebrate classes. *J Comp Neurol* 521(6):1430–1448.
8. Burns JC, Corwin JT (2013) A historical to present-day account of efforts to answer the question: "What puts the brakes on mammalian hair cell regeneration?". *Hear Res* 297:52–67.
9. Collado MS, et al. (2011) The postnatal accumulation of junctional E-cadherin is inversely correlated with the capacity for supporting cells to convert directly into sensory hair cells in mammalian balance organs. *J Neurosci* 31(33):11855–11866.
10. Harris JA, et al. (2003) Neomycin-induced hair cell death and rapid regeneration in the lateral line of zebrafish (Danio rerio). *J Assoc Res Otolaryngol* 4(2):219–234.
11. Williams JA, Holder N (2000) Cell turnover in neuromasts of zebrafish larvae. *Hear Res* 143(1-2):171–181.
12. Dufourcq P, et al. (2006) Mechano-sensory organ regeneration in adults: The zebrafish lateral line as a model. *Mol Cell Neurosci* 33(2):180–187.
13. Grant KA, Raible DW, Piotrowski T (2005) Regulation of latent sensory hair cell precursors by glia in the zebrafish lateral line. *Neuron* 45(1):69–80.
14. Nuñez VA, et al. (2009) Postembryonic development of the posterior lateral line in the zebrafish. *Evol Dev* 11(4):391–404.
15. Hirose K, Shimoda N, Kikuchi Y (2011) Expression patterns of lgr4 and lgr6 during zebrafish development. *Gene Expr Patterns* 11(7):378–383.
16. Kim SH, et al. (2010) Zebrafish type XVII collagen: Gene structures, expression profiles, and morpholino "knock-down" phenotypes. *Matrix Biol* 29(7):629–637.
17. Rohner N, et al. (2009) Duplication of fgfr1 permits Fgf signaling to serve as a target for selection during domestication. *Curr Biol* 19(19):1642–1647.
18. Behra M, et al. (2012) Transcriptional signature of accessory cells in the lateral line, using the Tnk1bp1:EGFP transgenic zebrafish line. *BMC Dev Biol* 12:6.
19. Gallardo VE, Behra M (2013) Fluorescent activated cell sorting (FACS) combined with gene expression microarrays for transcription enrichment profiling of zebrafish lateral line cells. *Methods* 62(3):226–231.
20. Gallardo VE, et al. (2010) Molecular dissection of the migrating posterior lateral line primordium during early development in zebrafish. *BMC Dev Biol* 10:120.
21. Parinov S, Kondrichin I, Korzh V, Emelyanov A (2004) Tol2 transposon-mediated enhancer trap to identify developmentally regulated zebrafish genes in vivo. *Dev Dyn* 231(2):449–459.
22. Wibowo I, Pinto-Teixeira F, Satou C, Higashijima S, López-Schier H (2011) Compartmentalized Notch signaling sustains epithelial mirror symmetry. *Development* 138(6): 1143–1152.
23. Mirkovic I, Pylawka S, Hudspeth AJ (2012) Rearrangements between differentiating hair cells coordinate planar polarity and the establishment of mirror symmetry in lateral-line neuromasts. *Biol Open* 1(5):498–505.
24. Ghysen A, Dambly-Chaudière C (2007) The lateral line microcosmos. *Genes Dev* 21(17): 2118–2130.
25. López-Schier H, Hudspeth AJ (2006) A two-step mechanism underlies the planar polarization of regenerating sensory hair cells. *Proc Natl Acad Sci USA* 103(49):18615–18620.
26. Villablanca EJ, et al. (2006) Control of cell migration in the zebrafish lateral line: Implication of the gene "tumour-associated calcium signal transducer," tacstd. *Dev Dyn* 235(6):1578–1588.
27. Haas P, Gilmour D (2006) Chemokine signaling mediates self-organizing tissue migration in the zebrafish lateral line. *Dev Cell* 10(5):673–680.
28. Xiao T, Roeser T, Staub W, Baier H (2005) A GFP-based genetic screen reveals mutations that disrupt the architecture of the zebrafish retinotectal projection. *Development* 132(13):2955–2967.
29. Matsuda M, et al. (2013) Lef1 regulates Dusp6 to influence neuromast formation and spacing in the zebrafish posterior lateral line primordium. *Development* 140(11): 2387–2397.
30. McGraw HF, et al. (2011) Lef1 is required for progenitor cell identity in the zebrafish lateral line primordium. *Development* 138(18):3921–3930.
31. Valdivia LE, et al. (2011) Lef1-dependent Wnt/β-catenin signalling drives the proliferative engine that maintains tissue homeostasis during lateral line development. *Development* 138(18):3931–3941.
32. Muto A, et al. (2005) Forward genetic analysis of visual behavior in zebrafish. *PLoS Genet* 1(5):e66.
33. Head JR, Gacioch L, Pennisi M, Meyers JR (2013) Activation of canonical Wnt/β-catenin signaling stimulates proliferation in neuromasts in the zebrafish posterior lateral line. *Dev Dyn* 242(7):832–846.
34. Wada H, et al. (2013) Wnt/Dkk negative feedback regulates sensory organ size in zebrafish. *Curr Biol* 23(16):1559–1565.
35. Kozlowski DJ, Whitfield TT, Hukriede NA, Lam WK, Weinberg ES (2005) The zebrafish dog-eared mutation disrupts eya1, a gene required for cell survival and differentiation in the inner ear and lateral line. *Dev Biol* 277(1):27–41.
36. Lan X, et al. (2011) Comparative analysis of duplicated sox21 genes in zebrafish. *Dev Growth Differ* 53(3):347–356.
37. Sahly I, Andermann P, Petit C (1999) The zebrafish eya1 gene and its expression pattern during embryogenesis. *Dev Genes Evol* 209(7):399–410.
38. Hernández PP, Moreno V, Olivari FA, Allende ML (2006) Sub-lethal concentrations of waterborne copper are toxic to lateral line neuromasts in zebrafish (Danio rerio). *Hear Res* 213(1-2):1–10.
39. Hernández PP, Olivari FA, Sarrazin AF, Sandoval PC, Allende ML (2007) Regeneration in zebrafish lateral line neuromasts: Expression of the neural progenitor cell marker sox2 and proliferation-dependent and-independent mechanisms of hair cell renewal. *Dev Neurobiol* 67(5):637–654.
40. Li S, et al. (2012) Foxp1/4 control epithelial cell fate during lung development and regeneration through regulation of anterior gradient 2. *Development* 139(14):2500–2509.
41. Ramachandran R, Zhao XF, Goldman D (2012) Insm1a-mediated gene repression is essential for the formation and differentiation of Müller glia-derived progenitors in the injured retina. *Nat Cell Biol* 14(10):1013–1023.
42. Liang J, et al. (2012) The stat3/socs3a pathway is a key regulator of hair cell regeneration in zebrafish. [corrected]. *J Neurosci* 32(31):10662–10673.
43. Katoh M (2012) Function and cancer genomics of FAT family genes (review). *Int J Oncol* 41(6):1913–1918.
44. Mahoney PA, et al. (1991) The fat tumor suppressor gene in Drosophila encodes a novel member of the cadherin gene superfamily. *Cell* 67(5):853–868.
45. Bryant PJ, Huettner B, Held LI, Jr., Ryerse J, Szidonya J (1988) Mutations at the fat locus interfere with cell proliferation control and epithelial morphogenesis in Drosophila. *Dev Biol* 129(2):541–554.
46. May-Simera H, Kelley MW (2012) Planar cell polarity in the inner ear. *Curr Top Dev Biol* 101:111–140.
47. Saburi S, et al. (2008) Loss of Fat4 disrupts PCP signaling and oriented cell division and leads to cystic kidney disease. *Nat Genet* 40(8):1010–1015.
48. Sopko R, McNeill H (2009) The skinny on Fat: An enormous cadherin that regulates cell adhesion, tissue growth, and planar cell polarity. *Curr Opin Cell Biol* 21(5):717–723.
49. Burgess HA, Johnson SL, Granato M (2009) Unidirectional startle responses and disrupted left-right co-ordination of motor behaviors in robo3 mutant zebrafish. *Genes Brain Behav* 8(5):500–511.
50. Challa AK, McWhorter ML, Wang C, Seeger MA, Beattie CE (2005) Robo3 isoforms have distinct roles during zebrafish development. *Mech Dev* 122(10):1073–1086.
51. Chen Z, Gore BB, Long H, Ma L, Tessier-Lavigne M (2008) Alternative splicing of the Robo3 axon guidance receptor governs the midline switch from attraction to repulsion. *Neuron* 58(3):325–332.
52. Ypsilanti AR, Zagar Y, Chédotal A (2010) Moving away from the midline: New developments for Slit and Robo. *Development* 137(12):1939–1952.
53. Bauer K, Dowejko A, Bosserhoff AK, Reichert TE, Bauer R (2011) Slit-2 facilitates interaction of P-cadherin with Robo-3 and inhibits cell migration in an oral squamous cell carcinoma cell line. *Carcinogenesis* 32(6):935–943.
54. Wong GK, Baudet ML, Norden C, Leung L, Harris WA (2012) Slit1b-Robo3 signaling and N-cadherin regulate apical process retraction in developing retinal ganglion cells. *J Neurosci* 32(1):223–228.
55. Schuck JB, et al. (2011) Transcriptomic analysis of the zebrafish inner ear points to growth hormone mediated regeneration following acoustic trauma. *BMC Neurosci* 12:88.
56. Cressman DE, Diamond RH, Taub R (1995) Rapid activation of the Stat3 transcription complex in liver regeneration. *Hepatology* 21(5):1443–1449.
57. Wenemoser D, Lapan SW, Wilkinson AW, Bell GW, Reddien PW (2012) A molecular wound response program associated with regeneration initiation in planarians. *Genes Dev* 26(9):988–1002.
58. Goley ED, Welch MD (2006) The ARP2/3 complex: An actin nucleator comes of age. *Nat Rev Mol Cell Biol* 7(10):713–726.
59. Singh RD, et al. (2013) Prominin-2 expression increases protrusions, decreases caveolae and inhibits Cdc42 dependent fluid phase endocytosis. *Biochem Biophys Res Commun* 434(3):466–472.
60. Varga M, et al. (2013) Autophagy is required for zebrafish caudal fin regeneration. *Cell Death Differ*, 10.1038/cdd.2013.175.
61. Jiang L, Romero-Carvajal A, Haug JS, Seidel CW, Piotrowski T (2014) Gene-expression analysis of hair cell regeneration in the zebrafish lateral line. *Proc Natl Acad Sci USA* 111:E1383–E1392.
62. Westerfield M (1993) *The Zebrafish Book: A Guide for the Laboratory Use of Zebrafish (Brachydanio rerio)* (Univ of Oregon Press, Eugene, OR).
63. Kwan KM, et al. (2007) The Tol2kit: A multisite gateway-based construction kit for Tol2 transposon transgenesis constructs. *Dev Dyn* 236(11):3088–3099.
64. Moens C (2008) Whole mount RNA in situ hybridization on zebrafish embryos: hybridization. *CSH Protoc*, 10.1101/pdb.prot5036.
65. Andersen CL, Jensen JL, Ørntoft TF (2004) Normalization of real-time quantitative reverse transcription-PCR data: A model-based variance estimation approach to identify genes suited for normalization, applied to bladder and colon cancer data sets. *Cancer Res* 64(15):5245–5250.
66. Casadei R, et al. (2011) Identification of housekeeping genes suitable for gene expression analysis in the zebrafish. *Gene Expr Patterns* 11(3-4):271–276.
67. Hortopan GA, Dinday MT, Baraban SC (2010) Spontaneous seizures and altered gene expression in GABA signaling pathways in a mind bomb mutant zebrafish. *J Neurosci* 30(41):13718–13728.

Supporting Information

Steiner et al. 10.1073/pnas.1318692111

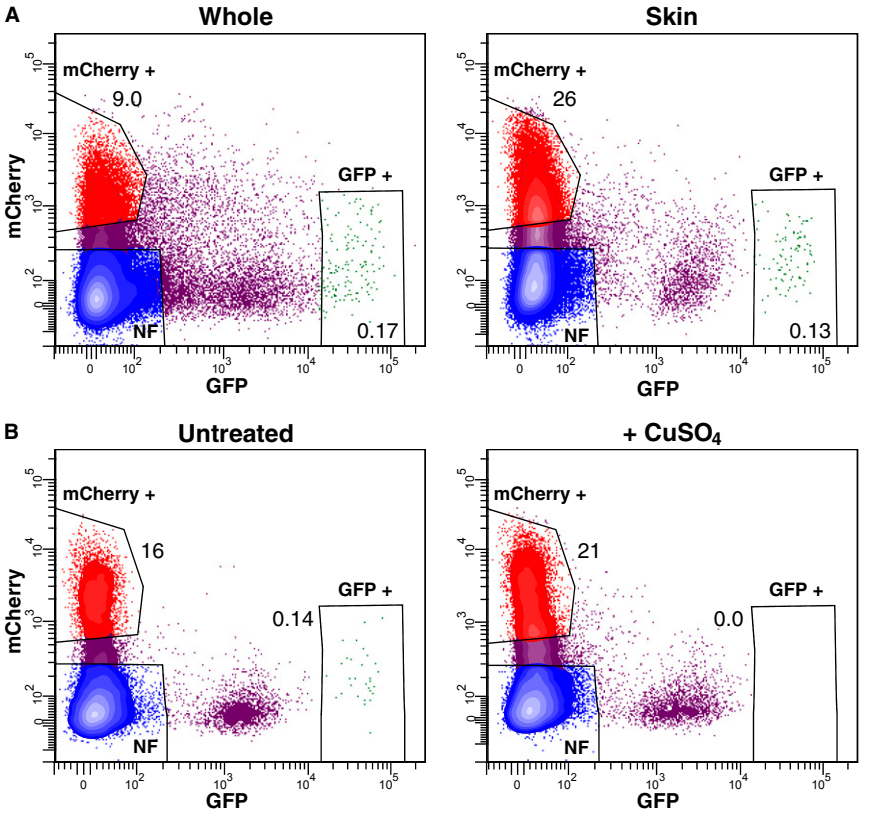

Fig. S1. (*A*) Using only dissected skins improves the relative yield and purity of sorted cells. Four whole *alpl:mCherry;pou4f3:GFP* larvae or 40 skins were dissociated and their cells subjected to flow cytometry. Probability-contour plots demonstrate that skins alone (*Right*) produce clearer separation of cell types, particularly hair cells, and increase the relative yield of mCherry-positive and GFP-negative (mCh^+) mantle cells than whole larvae (*Left*). (*B*) Treatment with $CuSO_4$ effectively and specifically destroys hair cells. The *alpl:mCherry;pou4f3:GFP* larvae were treated with 5 μM $CuSO_4$ for 1 h. One hour later, their skins were dissected and dissociated for flow-cytometric analysis alongside those of untreated controls. GFP-positive and mCherry-negative (GFP^+) hair cells were completely eliminated; for about 120,000 total events in each experiment, there were no cells after treatment vs. 30 in controls. In contrast, numbers of mCh^+ cells were relatively unaffected; these cells represented 4.3% of total events after $CuSO_4$ treatment vs. 2.9% in controls. Numbers in plots represent the percentage of total singlet particles within each associated gate.

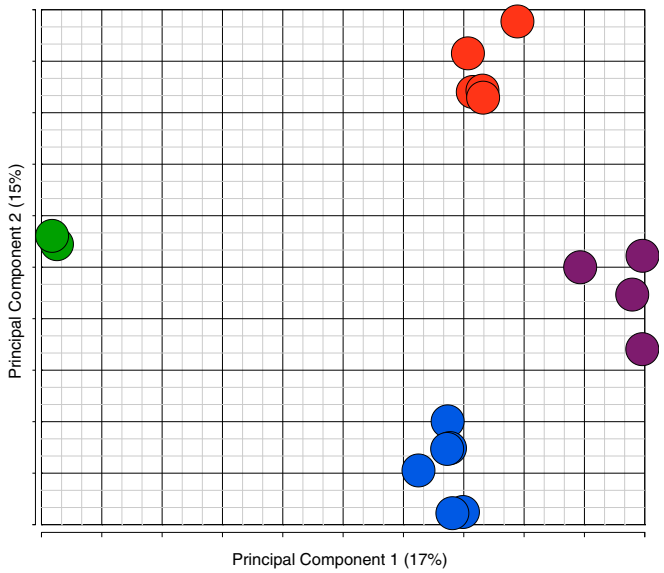

Fig. S2. Principal-component analysis demonstrates the high similarity of biological replicates used for microarray analysis. The abscissa represents the greatest source of variance between samples and the ordinate represents the second-greatest. Each circle represents the results of one microarray hybridization. Green dots represent GFP^+ hair-cell samples, red dots represent mCh^+ samples, blue dots represent nonfluorescent (NF) samples from *alpl:mCherry*; *pou4f3:GFP* larvae, and purple dots represent mCh^+/GFP^+ samples from *alpl:mCherry*;*Et20* larvae. Clustering of dots of the same color indicates that there is less variance between samples of the same character than between distinct samples. The two greatest principal components account for 32% of the variance between samples.

Table S1. Primer sets for amplifying in situ hybridization probes and sources for other probe templates

Gene name	Gene symbol	Ensembl accession no.	In situ primer pair (5′-3′) or source of construct
Angiopoietin 2b	*angpt2*	ENSDART 00000076023	B. Weinstein (National Institutes of Health)
C1q and tumor necrosis factor-related protein 5	*c1qtnf5*	ENSDART 00000078570	GCACTGCTCGTTTCTCTTTCGCCT/AACGGGCACACCGTGGCTTC
Esophageal cancer-related gene 4a	*ecrg4a*	ENSDART 00000078523	ATGCTTTCTGAAAAGTTTCACCTGCATC/TCTTGTTGGCATCGGTGACGTG
FAT tumor suppressor homolog1a	*fat1a*	ENSDART 00000103262	L. Goodrich (Harvard University)
FAT tumor suppressor homolog 1b	*fat1b*	ENSDART 00000011953	L. Goodrich (Harvard University)
Fibroblast growth factor receptor 1a	*fgfr1a*	ENSDART 00000074774	ACCTCGTTCCACTGGTTGAC/ACGTCCAGCTGGTATGTGTG
Fibronectin type III domain containing 7	*fndc7*	ENSDART 00000142938	TTGTCCCTGCTAGGCAACAG/TGTTGCAGACTCCGTTGTGA
Germ cell-specific gene 1-like	*gsg1l*	ENSDART 00000054408	CTGTCGTTTCGGGCCGGTGA/TGCGGCGAAGGCGTTCAGTT
4-Hydroxyphenylpyruvate dioxygenase b	*hpdb*	ENSDART 00000066050	Open Biosystems, Inc.; Mammalian Gene Collection: 92456
Metastasis suppressor 1-like	*mtssl1a*	ENSDART 00000124075	CGCGTCTCGGTCCTCTGGTG/TGGCGGCTATAGTGGCCGGG
Phenylalanine hydroxylase	*pah*	ENSDART 00000011943	Zebrafish International Resource Center, EST/cDNA cb877
Phosphate-regulating gene with homologues to endopeptidases on the X chromosome	*phex*	ENSDART 00000090010	CGGTGGACCCGTGCGATGAC/CCCAGCGAGGGGTCAGAGAGG
Pentraxin 3, long a	*ptx3a*	ENSDART 00000098673	CGACGGGCCGGGACTCAAAC/ACGCACAAAGGTGCCCCCAC
Roundabout homolog 3	*robo3*	ENSDART 00000024778	C. Beattie (Ohio State University)
Tetraspanin 1	*tspan1/net1*	ENSDART 00000073757	GGCATATGTGTGGCTACCGT/GCAGTGACTCCAGCAGCTAT
Uncoupling protein 1	*ucp1*	ENSDART 00000038807	ATGGTGGGTCTGAAGCCGTC/CTACGCAGCGGCTTCGATTC

Table S2. Primer sets used for quantitative PCR analysis

Gene name	Gene symbol	Ensembl or GenBank accession no.	Quantitative PCR primer pair (5′-3′)	Length, bp
Actin-related protein 2/3 complex subunit 1a	*arpc1a*	NM_001002100	CTTGTGCCTCGGACAGGAAT/TGTTCTCAAGAGGCGACCAC	123
Autophagy-related protein 2 homolog B-like	*atg2bl*	XM_001340472	CCCATGTGCTGGTCCAGTTT/GGCTGAAAGCTCTCTCCCTG	98
Bloodthirsty-related gene family, member 4	*btr04*	ENSDART 00000102320	TAGGTTTTTCCACGCTCACGA/CCTCAAACAGAGGACCCTGG	152
FAT tumor suppressor homolog 2	*fat2*	ENSDART 00000014149	CTCGCTTCGGAGGTTTTCCT/GTCCGTCAGGCCCTAAGAAG	108
Fibroblast growth factor receptor 1a	*fgfr1a*	ENSDART 00000074774	CTGCCATATGTCCGAGCCTT/GTGATGGGAGTGGCCGATAG	144
Fibronectin type III domain containing 7	*fndc7*	XM_002660888	ACCAGCTGTATCCTCCCAGT/GGATCAGTGATGGCAGTGCT	98
Krüppel-like factor 3	*klf3*	ENSDART 00000014916	CCACAGCCAAGAGAAATCGGTC/GTGTGCGTCTATGGGCTTTCAG	182
Lectin, galactoside-binding, soluble, 1 (galectin 1)-like 1	*lgals1l1*	ENSDART 00000141904	TGTGCATTTCATTGCTTTGCTG/TTTAGACAGGCAGTGCCACA	120
Prominin 2	*prom2*	ENSDART 00000136318	TTCTTGGAGTGGCGTTTTGC/GGTCAGCTGGGACTGTGTTT	121
Tetraspanin 1	*tspan1/net1*	ENSDART 00000073757	CGTAGGGATATGGGCGACTG/TGCGCCAATACAGATGCAGA	115
Reference genes				
Cysteine and tyrosine-rich protein 1	*cyyr1*	NM_212882	GTGCTGTCAGGAACGGCTAT/CTTCACACACATGCAGACGC	99
Elongation factor 1	*ef1a*	NM_131263	CTGCCAGTGTTGCCTTCGT/CCTTGCGCTCAATCTTCCA	105
Solute carrier family 25 alpha, member 5	*slc25a5*	NM_173247	GTGTCCGTGCAGGGTATCAT/ACAGCAGTCACACTCTGAGC	134
β-Actin 1	*βact-1*	AF057040	CATCCATCGTTCACAGGAAGG/TGGTCGTTCGTTTGAATCTCAT	83
β-Actin 2	*βact-2*	NM_181601	TTACCACTTCACGCCGACTC/GTCACCTTCACCGTTCCAGT	117

Other Supporting Information Files

Dataset S1–S4 (XLSX)